Part 4

Energy – Fuel Cell and Electrolytes Materials

CO_2 separation membranes: innovative combination of known materials

S. G. Patrício[1]
A. I. B. Rondão[1]
A. Jamale[1]
N. Martins[1]
F. M. B. Marques[1]

Abstract

Standard electrolyte materials (ceramic oxide-ion conductors and eutectic mixtures of alkaline carbonates) used in Solid Oxide and Molten Carbonate Fuel Cell technologies can be combined to produce composite CO_2 separation membranes for a variety of applications. The model performance of these membranes is reviewed highlighting critical design and performance parameters. This model is used to build diagrams where actual membrane permeation data can be benchmarked against an ideal performance, providing immediate guidance on likely kinetic limitations. A complementary pictorial tool is also described to assess the electrical microstructure of these composites before permeation tests. The added value from combination of such diagrams in process control or membrane development is discussed.

Keywords: CO_2 separation membranes; ambipolar conductivity; electrical microstructure; performance benchmarking.

1. Introduction

Hydrogen as fuel is essential for the production of electrical power using environmental friendly systems like fuel cells. Hydrogen energy is expected to play a key role in a sustainable development scenario. However, while a rather abundant element, the obvious sources for hydrogen are molecules where this element is

1 Department of Materials and Ceramic Engineering, CICECO University of Aveiro, 3810-193 Aveiro, Portugal

strongly bonded. Water electrolysis using electrical power from renewable sources is a possible solution for the production of hydrogen but other solutions can also be envisaged, namely starting from bio-fuels like ethanol. Examples of integrated hydrogen energy/production solutions are depicted in Figure 1.

When hydrogen is combined with carbon, as in bio-fuels, the maximum hydrogen yield will produce carbon dioxide as side product. The same is true when using hydrocarbons. Standard processing steps in the conversion to hydrogen are the partial oxidation and the water-gas shift reactions, so that tentatively all hydrogen involved will be released as free molecules while all carbon will be converted to CO_2. Separation of H_2 from CO_2 can be obtained using selective separation techniques for any of these species. Separation of CO_2 from flue gases is also an urgently needed technology to ensure efficient capture of this deleterious compound while fossil fuels play a relevant role in the power production scenario.

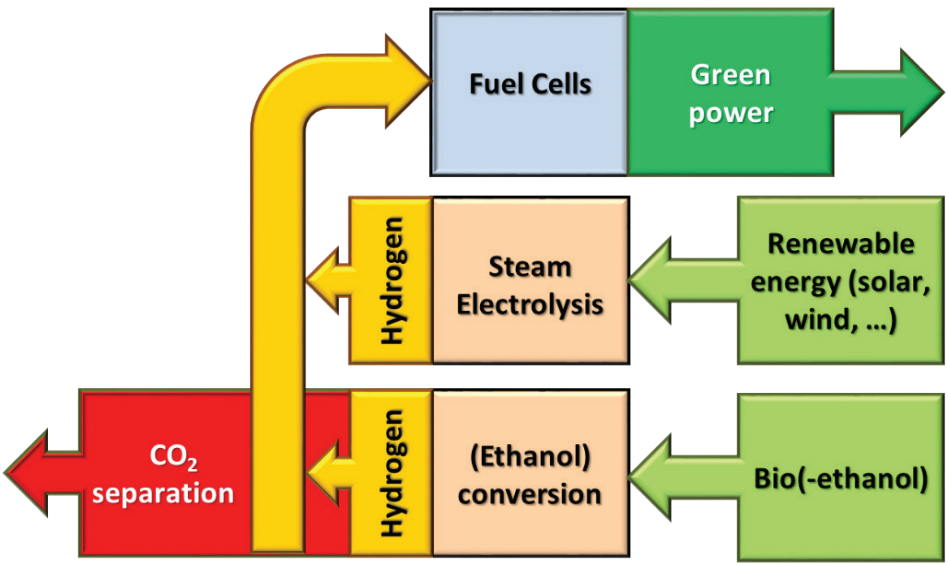

Figure 1 Scheme showing complementary solutions involving sustainable hydrogen production as source of green electrical power from fuel cells.

Composite membranes based on ceramic electrolytes (often Sm or Gd-doped, SDC or CGO) and eutectic mixtures of alkaline carbonates (e.g., K, Na and Li) can be used in CO_2 separation, fuel cells, steam electrolysis or even electrochemical synthesis of ammonia [1-7]. These composites combine standard materials used in Solid Oxide Fuel Cells (SOFCs) and Molten Carbonate Fuel Cells (MCFCs). While the SOFC ceramic electrolytes are well established oxide-ion conductors, the MCFC alkaline carbonates are described either as

dominant carbonate or alkaline ion conductors [8-13]. Most descriptions of these materials as constituents of CO_2 separation membranes consider that the dominant ionic charge carriers are oxide and carbonate ions. Here the same simplified assumption will be adopted.

Processing of composite CO_2 separation membranes can benefit from the state of the art knowledge in SOFC and MCFC technologies. Laboratory scale tests exploited both flat and tubular cell configurations, thin and thick electrolyte layers (supported on substrates or self-supported), all concepts usual in fuel cell systems. However, the efficient combination of electrolyte materials from technologies with distinct envisaged working temperatures has obvious constraints, namely the chemical stability between several oxide systems and molten carbonate phases, and uneven electrical conductivities under typical operational conditions (500-700 °C).

In composite CO_2 separation membranes the flow of carbonate ions is balanced by counter flow of oxide ions, as such yielding net flow of CO_2, as depicted in Figure 2. In such circumstances, the slowest charge carrier (poor conductor) will be rate determining with respect to performance. Since charge transport in both phases shows markedly distinct characteristics this must be taken into consideration for proper membrane design (e.g., selected materials, phase percentages, microstructures, working temperatures). In fact, typical eutectic mixtures of alkaline carbonates possess electrical conductivity in excess of 0.1 S/cm already at 500 °C while usual ceramic electrolytes only reach such values at 800 °C [14-17].

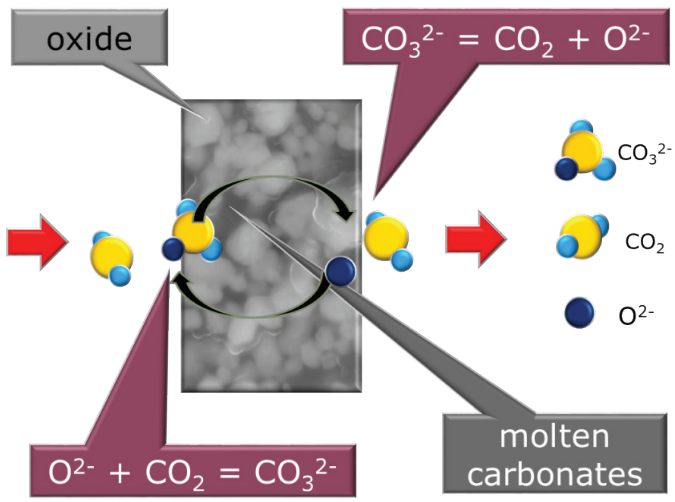

Figure 2 Scheme of the operating principle of a composite CO_2 separation membrane. The counter flow of carbonate and oxide ions inside the membrane (via molten carbonates and oxide phases, respectively) explains the selective separation process.

The present work starts with the revision of a model on membrane permeation, to highlight critical design parameters [18-21]. In a second part of this work, the role of the composite microstructure on the membrane performance is also reviewed [22]. Both approaches are used to introduce two distinct diagrams where distinct membrane characteristics can be plotted, providing immediate information on likely reasons for modest operation. Used in a complementary manner, these two diagrams provide unique benchmarking tools that can be applied in the control or development of materials and actual membranes for CO_2 separation.

2. Model membrane performance

2.1 Equivalent circuit

Electrolyte-based cells can be properly described by equivalent electrical circuits. Figure 3 shows a global scheme of the simplified equivalent circuit used to describe the composite membrane performance [21]. We have two cells (MC/molten carbonates, and SO/solid oxide) with ionic branches accounting for the ionic transport inside the cells (I_j, with j=MC or SO), with ionic resistors (R_i) and cell thermodynamic voltages ($V_{o,j}$) as main circuit elements.

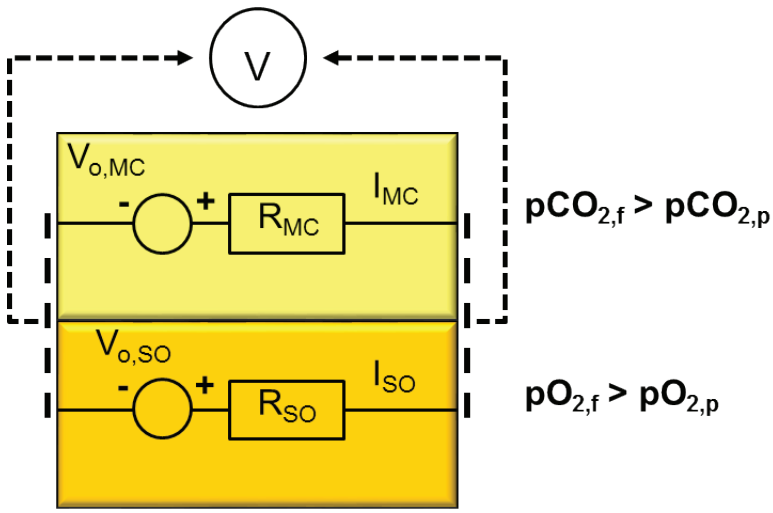

Figure 3 Simplified equivalent circuit used to describe the performance of a CO_2 separation membrane. See text for the meaning of the symbols.

The following reactions can be assumed for the molten carbonates and solid oxide cells, respectively:

$$CO_2 + ½\ O_2 + 2\ e^- \leftrightarrows CO_3^= \quad (1)$$

$$½\ O_2 + 2\ e^- \leftrightarrows O^= \quad (2)$$

At the membrane feed side forward reaction (1) is combined with reversed reaction (2) ($CO_2 + O^= \rightarrow CO_3^=$). At the membrane permeate side we have the opposite combination ($CO_3^= \rightarrow CO_2 + O^=$). Accordingly, we have no net flow of electrons or molecular oxygen.

The oxide and the carbonates experience distinct thermodynamic voltages ($V_{o,j}$), driven by the free energy changes in the cell reactions just presented. We can express them as:

$$V_{o,MC} = \frac{RT}{2F}.\ln\frac{pCO_{2,f}}{pCO_{2,p}} + \frac{RT}{4F}.\ln\frac{pO_{2,f}}{pO_{2,p}} \quad (3)$$

$$V_{o,SO} = \frac{RT}{4F}.\ln\frac{pO_{2,f}}{pO_{2,p}} \quad (4)$$

Where pO_2 and pCO_2 correspond to the partial pressures of oxygen and carbon dioxide in the gas phase, used here instead of the corresponding activities. The subscripts f and p refer to the distinct membrane boundary conditions (feed and permeate sides, respectively); R and T have their usual meanings.

For a gas rich in CO_2 (e.g., >10 vol%) and with a modest O_2 content of only a few percent (e.g., below 2%) in the membrane permeate side, we would have gradients with the same signal assuming low partial pressures of both gases in the permeate side due to light vacuum. However, we can only sustain a steady flow of carbonate ions from the feed side to the permeate side (forward reaction (1)) if we have a counter flow of oxide ions via the solid electrolyte (reaction (2) backwards). This means that the molten carbonates cell is running in galvanic mode while the solid oxide cell is running in electrolytic mode. Assuming dominant ohmic losses in both cells, the corresponding individual cell voltages (V_{MC} and V_{SO}) are:

$$V_{MC} = V_{o,MC} - |I_{MC}|.R_{MC} \quad (5)$$

$$V_{SO} = V_{o,SO} + |I_{SO}|.R_{SO} \quad (6)$$

From analysis of the equivalent circuit shown in Figure 3, the working voltages and currents (V and I) in both cells must be the same:

$$V = V_{MC} = V_{SO} \tag{7}$$

$$I = |I_{MC}| = |I_{SO}| \tag{8}$$

Combining equations (3) through (8), we can express I as a function of the membrane boundary conditions and the partial solid oxide and molten carbonates conductivities ($s_{p,j}$) in the membrane:

$$I = \frac{RT}{2F(R_{MC}+R_{SO})} \ln\left(\frac{pCO_{2,f}}{pCO_{2,p}}\right) = \frac{SRT.\sigma_{p,MC}.\sigma_{p,SO}}{2Fd.(\sigma_{p,MC}+\sigma_{p,SO})} \ln\left(\frac{pCO_{2,f}}{pCO_{2,p}}\right) \tag{9}$$

The resistances (R_j) and conductivities (s_j) of both phases are related as usual by $R_j = d/s_j.S$, with S and d being the membrane surface area and thickness, respectively. The ambipolar conductivity of the composite ($s_{p,SO}.s_{p,MC}/(s_{p,SO}+s_{p,MC})$) depends on constituent phases (composition), corresponding volume fractions, microstructure and working temperature. The cell current can be expressed as a function of the volume fraction of both phases and their nominal conductivities as pure phases:

$$I = \frac{SRT.(1-\chi)\sigma_{MC}.\chi\sigma_{SO}}{2Fd.[(1-\chi)\sigma_{MC}+\chi\sigma_{SO}]} .\ln\left(\frac{pCO_{2,f}}{pCO_{2,p}}\right) \tag{10}$$

In this equation is the solid oxide volume fraction and the partial conductivity of each phase was assumed as a direct function of the pure phase conductivity weighted by the corresponding volume fraction (e.g., $s_{p,SO}=\chi.s_{SO}$). Conversion of current into CO_2 molar permeation flux (=I/2FS), and consideration of the tortuosity (τ) effect on ionic transport yields:

$$J_{CO_2} = \frac{RT}{4F^2 d} \frac{1}{\tau} \sigma_{amb} \ln \frac{pCO_{2,f}}{pCO_{2,p}} \tag{11}$$

In eq. (11) tortuosity was introduced as global parameter. Distinct tortuosity factors might also be considered for each phase [18-20].

2.2 A schematic diagram of membrane performance

The diagram presented in Figure 4 shows the dependence of the two cell voltages on the membrane internal current. Based on the assumed membrane

boundary conditions the voltage described by equation (3) is larger than the voltage estimated by equation (4), which explains the relative positions of $V_{o,MC}$ and $V_{o,SO}$, the thermodynamic voltages that would be experienced independently by each phase if exposed to the mentioned boundary conditions.

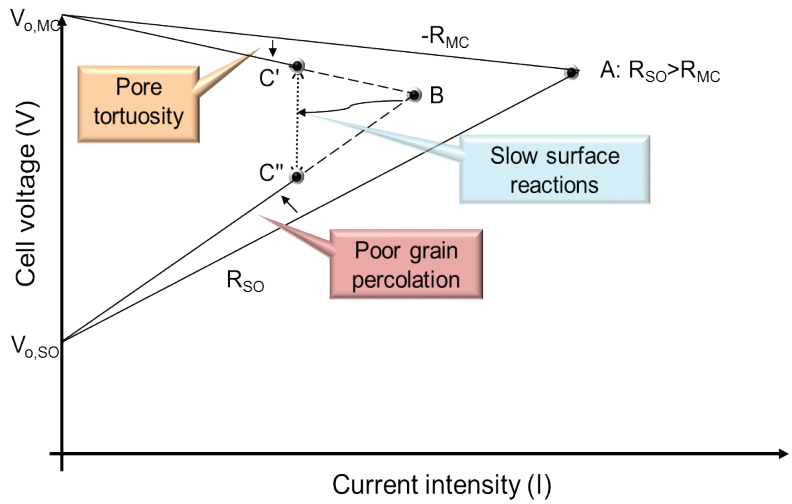

Figure 4 Schematic diagram on the performance of CO_2 separation membranes highlighting three possible operating conditions described as points A, B, and C′/C″. A corresponds to an ideal performance, that can be used for benchmarking. B shows an operating condition where microstructural constraints are relevant. In C′/C″ slow surface kinetics is responsible for a significant voltage drop. See text for further details.

For the molten carbonates, the larger the current the lower the cell voltage (equation (5)). For the solid electrolyte, a voltage larger than the cell open circuit voltage is needed (equation (6)). Lines departing from $V_{o,MC}$ and $V_{o,SO}$ might meet at points like A or B. Each point corresponds to a current/condition determined by the boundary conditions and inner cell resistances.

Point A in Figure 4 might correspond to an ideal membrane performance (perfect microstructure, no surface kinetic limitations) where the CO_2 permeation rate is governed by the high solid oxide resistance. This ideal performance can be determined from literature data [14-17] and established gas boundary conditions, using equation (10), and can be used for benchmarking purposes. Point B corresponds to a hypothetical situation derived from point A where we have significant microstructural constraints, namely poor percolation of oxide grains and high tortuosity throughout the molten carbonates phase. Such features will impact (increase) the actual ionic resistances of both phases, determining the shift of the corresponding cell lines to new positions, as indicated by the small arrows.

The impact of slow surface kinetics is introduced in a schematic manner, starting from point B as reference. Slow surface/interface steps of any type will

displace the working condition from point B to the left in the diagram, as in the couple C'/C". The vertical line between C' and C" can be understood as an overpotential with origin in the mentioned kinetic constraints (e.g., gas concentration polarization).

This type of diagram can indeed be used to map the performance of actual membranes against an ideal working condition and to obtain further guidance on membrane design, as shown elsewhere [21]. In the case of ceria-based membranes with typical microstructures the performance might be slightly improved namely decreasing the tortuosity of oxide pores and improving the percolation of the grains of the oxide skeleton. However, decreasing membrane thickness is probably the most effective design parameter.

3. On the membrane "electrical microstructure"

The oxide-ion conductivity in pure and dense ceria-based electrolytes usually shows an almost constant activation energy but the lower temperature electrical performance depends strongly on microstructure. Ion-blocking grain boundaries are typical in most ceramic oxide-ion conductors. In composites, these may combine with constriction resistances due to poor necking between oxide particles, as shown in a schematic manner in case A, Figure 5(a).

Lightly bonded grains (light grey rounded particles), even hanging aside from the ceramic skeleton, are often found in co-fired samples (Figure 5(b)). In case B, Figure 5(a), the oxide phase percolation is improved, situation obtained when the ceramic backbone is fired before impregnation with the molten carbonates (dark grey jelly-like regions in Figure 5(b)-(d)). Indeed, pre-sintered backbones can be the source of rather regular microstructures (Figures 5(c) and (d)). These comments and examples are enough to highlight how diverse the backbone characteristics of distinct composites might be even with similar phase content.

While the situation for oxides is already quite complex, carbonates move from a poorly conducting solid at low temperature to a liquid with high conductivity when the eutectic temperature is reached. However, even in the liquid condition, isolated or poorly interconnected pools of alkaline carbonates are also possible. Pore tortuosity will increase the average length for ionic transport within the molten phase. In summary, the electrical contribution of each phase depends strongly on the microstructure. This explains the need to know in detail what is the "electrical microstructure" of a given composite, information hardly reached by simple microscopy.

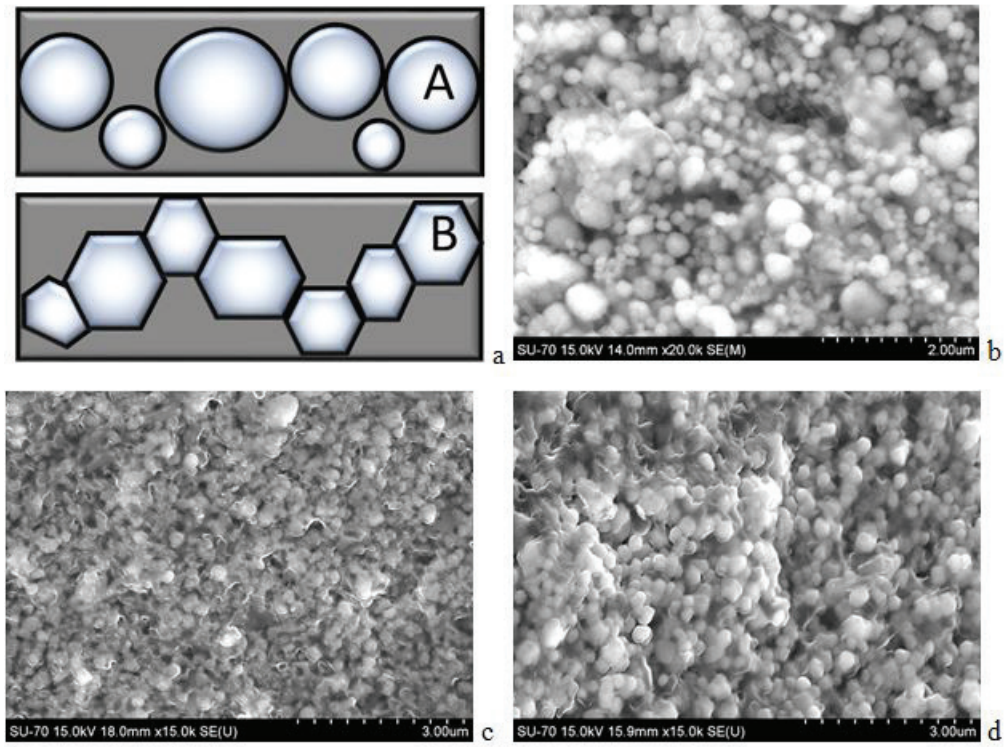

Figure 5 (a) Schematic drawing to highlight different percolation conditions within the ceramic phase in composite membranes; (b)-(d) Microstructures of composite membranes of Gd-doped ceria (CGO, about 70 vol%) and eutectic mixtures of Li and Na carbonates (LNC, about 30 vol%), jointly milled and co-fired (b) or from pre-sintered CGO backbones impregnated with LNC at 700 °C (c) and 800 °C (d), respectively.

While microstructural effects might influence the electrical performance of both phases in distinct manners, due to the contrasting electrical properties of oxide and alkaline carbonates at low and high temperature, the actual electrical contribution of each phase in composite membranes can be easily assessed using impedance spectroscopy. A meaningful ac equivalent circuit consisting of parallel branches related to each phase was previously tested with this goal [23-25].

Figure 6 includes typical sets of data obtained at low temperature, when the composite performance is governed by the oxide phase. Data obtained under distinct conditions (low and high temperature) or studying skeletons and composites in parallel, can be used to reveal the membrane "electrical microstructure" under typical working conditions. If the electrical microstructure of a composite membrane is indeed complex, impedance spectroscopy provides a quite simple route to quantify the electrical characteristics (resistances or partial conductivities) of both phases.

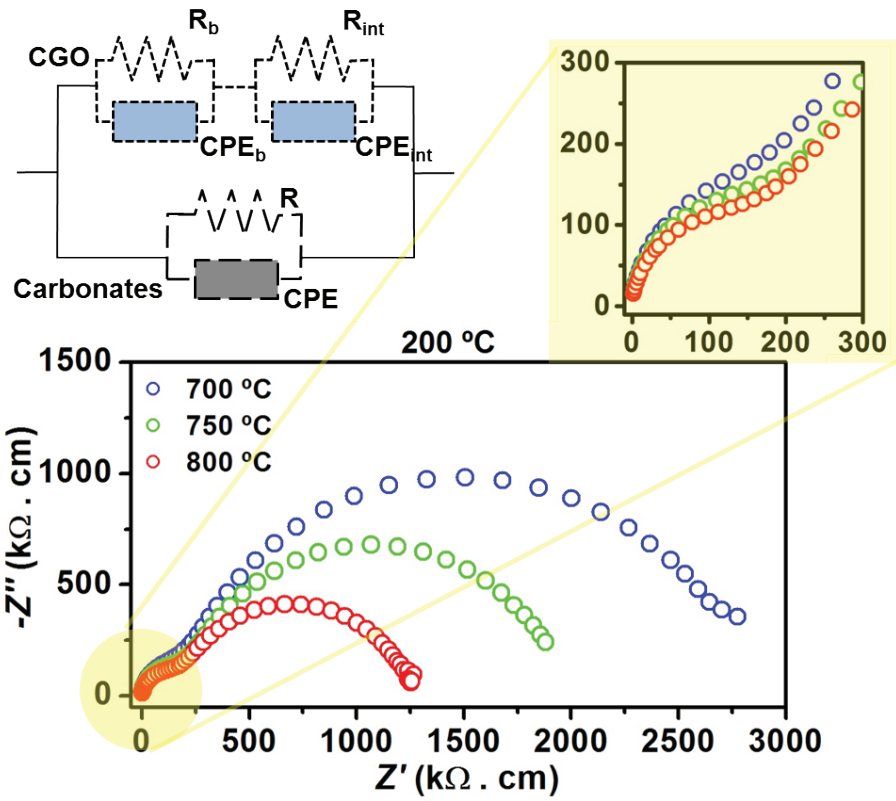

Figure 6 Examples of impedance spectra obtained with composite membranes (95 vol% CGO) obtained by co-firing of all phases, in air. As figure insets, the exploded view of the high frequency range of data and the assumed equivalent circuit used in data analysis. Circuit elements are R- resistor and CPE - constant phase element, while the subscripts stand for bulk (b) and interface (int).

Starting from here, assessing and benchmarking the electrical microstructure of composite membranes can benefit from an approach similar to the previously discussed solution for membrane permeation (Figure 4). In fact, ambipolar conductivity, already introduced, and ionic transport (or transference) numbers (defined as the ratio between the partial conductivity of a given ionic species and the total conductivity, $t_i=s_i/\Sigma s_i$) can be linked in one single diagram. The following text will be used to introduce this additional tool.

From definition, t_{SO} and t_{MC}, the ionic transport numbers of charge carriers in each phase, are:

$$t_{SO}=\frac{\sigma_{SO}}{\sigma_{SO}+\sigma_{MC}}=\frac{R_{MC}}{R_{SO}+R_{MC}} \qquad (12a)$$

$$t_{MC} = \frac{\sigma_{MC}}{\sigma_{SO}+\sigma_{MC}} = \frac{R_{SO}}{R_{SO}+R_{MC}} \quad (12b)$$

while R_{SO} and R_{MC} are the solid oxide and molten carbonate resistances that can be estimated from impedance spectroscopy data [22]. These same quantities can be used to estimate the ambipolar conductance of the membrane (G_{amb}), defined as:

$$G_{amb} = \frac{1}{(R_{MC}+R_{SO})} = \frac{S}{d} \cdot \frac{\sigma_{SO,p} \cdot \sigma_{MC,p}}{(\sigma_{SO,p}+\sigma_{MC,p})} \quad (13)$$

With the meaning of all symbols as previously introduced.

Linking of ionic transport numbers with ambipolar conductance can be reached in a diagram (Figure 7) where the vertical axis corresponds to t_{MC} and the horizontal axis is the ambipolar conductance of the membrane [22]. In drafted triangles, two vertices correspond to t_{MC}=1 and 0 and the third vertex (points A or B) corresponds to the membrane performance (G_{amb}, t_{MC}). The slope of the line from origin to (G_{amb}, t_{MC}) corresponds to the solid oxide resistance, R_{SO}. The slope of the line from t_{MC}=1 to (G_{amb}, t_{MC}) corresponds to -R_{MC}. The similarity between this and the previously introduced diagram is obvious. However, the first kind of diagram requires effective permeation measurements while the second diagram can be based on simpler impedance spectroscopy measurements.

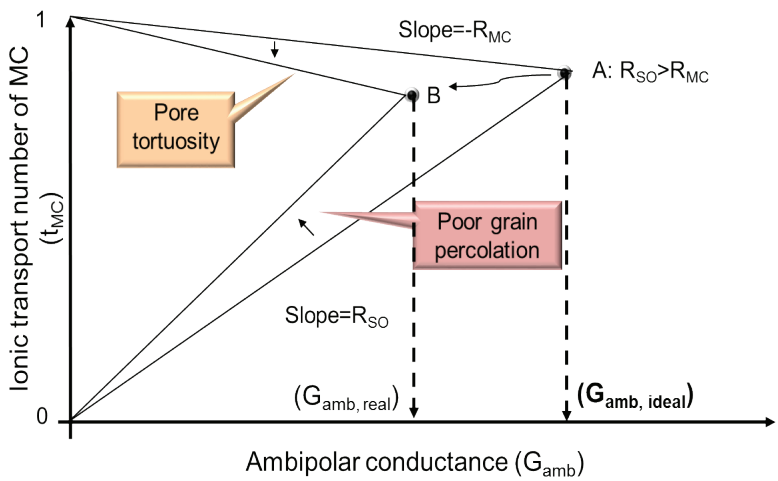

Figure 7 Schematic diagram used to benchmark the electrical microstructure of composite membranes [22]. Point A corresponds to a hypothetical ideal performance (estimated from literature data) while points like B can be generated from impedance spectroscopy data. See text for details.

Ideal MC and SO lines can again be estimated from literature data, corresponding to the best electrical performance expected for membranes without any microstructural constraints (meeting in point A). Point B corresponds to a real membrane showing microstructural constraints. These two distinct conditions (A and B) and the associated ambipolar conductances were pinpointed as vertical arrows. The ratio between any real ambipolar conductance and the ideal performance for the same composition can be easily used to measure the microstructural electrical efficiency of a composite membrane.

4. Final remarks

Dual phase mixed ionic and electronic membranes for oxygen separation, also relying on ambipolar transport, reach maximum oxygen flows in the range of 1 $cm^3/cm^2.min$ [26]. Table 1 includes two typical results of CO_2 separation membranes, reported in the literature, for working temperatures in the order of 650 °C and a membrane thickness in the vicinity of 1 mm. As immediate conclusion from the analysis of these data, state of the art membrane permeation rates are not far distant from ideal values (around 70% of the theoretical value, see column I_{exp}/I_{th}), and should be easily brought to target values of 1 $cm^3/cm^2.min$ decreasing their thickness. This means that the potential of these membranes for practical systems is rather high.

Table 1 Typical examples of membrane performance at 650 °C.

Oxide phase	χ_{SO}	Carbonates	J_{CO2} ($cm^3/cm^2.min$)	I_{exp}/I_{th}	Ref.
Sm-doped ceria	0.5	Na and Li	0.123	0.76	[27]
Gd-doped ceria	0.73	Na and Li	0.236	0.67	[28]

J_{CO2} - flux of CO_2 across the membrane; I_{exp} - ionic current across the membrane; I_{th} - estimated ionic current using eq. (10) and literature data; χ_{SO} – volume fraction of SO.

The diagrams previously introduced to map the performance of composite membranes are of great value to identify permeation constraints and to monitor the membrane characteristics throughout the processing stage. In fact, simple impedance spectroscopy measurements can provide an immediate assessment on how suitable is the membrane microstructure, using diagrams like Figure 7. The exact membrane permeation, if plotted in diagrams like Figure 4, will further indicate the likely presence of surface/reaction kinetic limitations. The added value from a combination of both types of diagrams is clear. While the diagram focused on the electrical microstructure of the membrane is only effective for the assess-

ment of internal ionic transport, the second type of diagram is also influenced by surface reaction kinetics. Thus, the membrane microstructural optimization (or processing control) can be based on the simpler diagram and measurements. However, the design and assessment of the membrane/gas interface characteristics, playing a large role in kinetics, is only feasible using the second type of diagram and actual permeation measurements. These comments highlight how these aspects complement each other.

5. Conclusions

Combination of materials used in known fuel cell technologies can originate new functionalities of great significance in the field of energy production, namely composite CO_2 separation membranes. The state of the art performance of these composite membranes is closely reaching competitive values, while some design parameters (membrane thickness) are far from fully exploited. Adequate diagrams can be used to monitor the development of composite membranes, for quality control in production, or to obtain a valuable insight on kinetic constraints.

Acknowledgement

Funding from Projects NANOMFC - New-INDIGO/0001/2013, CO2zero – POCI-01-0145-FEDER-016654 (Ref. FCT PTDC/CTM-CER/6732/2014) and CICECO-Aveiro Institute of Materials - POCI-01-0145-FEDER-007679 (Ref. FCT UID/CTM/50011/ 2013), financed by national funds (Portugal) through FCT/MEC and when appropriate co-financed by FEDER under the COMPETE/PT2020 Partnership Agreement is greatly appreciated. S. Patrício and A. Rondão thank FCT for their grants (SFRH/BPD/75943/ 2011 and SFRH/BDE/52139/2013, respectively).

References

[1] K. POINTON, B. LAKEMAN, J. IRVINE, J. BRADLEY, S. JAIN, **The development of a carbon–air semi fuel cell,** J. Power Sources, 162 (2006) 750–756.

[2] B. ZHU, X. LIU, P. ZHOU, X. YANG, Z. ZHU, W. ZHU, **Innovative solid carbonate – ceria composite electrolyte fuel cells**, Electrochem. Comm., 3 (2001) 566-571.

[3] Y. LI, Z. RUI, C. XIA, M. ANDERSON, Y.S. LIN, **Performance of ionic-conducting ceramic/carbonate composite material as solid oxide fuel cell electrolyte and CO_2 permeation membrane**, Catal. Today, 148 (2009) 303-309.

[4] Z. RUI, M. ANDERSON, Y. LI, Y.S. LIN, **Ionic conducting ceramic and carbonate dual-phase membranes for carbon dioxide separation,** J. Membr. Sci, 417-418 (2012) 174-182.

[5] X. DONG, J.O. LANDEROS, Y. S. LIN, **An asymmetric tubular ceramic-carbonate dual phase membrane for high temperature CO_2 separation,** Chem. Commun., 49 (2013) 9654-9656.

[6] B. ZHU, I. ALBINSSON, C. ANDERSSON, K. BORSAND, M. NILSSON, B.-E. MELLANDER, **Electrolysis studies based on ceria-based composites,** Electrochem. Commun., 8 (2006) 495-498.

[7] I.A. AMAR, C.TG. PETIT, L. ZHANG, R. LAN, P.J. SKABARA, S. TAO, **Electrochemical synthesis of ammonia based on doped-ceria-carbonate composite electrolyte and perovskite cathode,** Solid State Ionics, 201 (2011) 94–100.

[8] R.L. FREDERICK, E.K. WILLIAMS, **^{23}Na and ^{14}C Diffusion in a Mixture of Li/Na/KCO_3,** J. Electrochem. Soc., 116 (1969) 454-455.

[9] P.L. SPEDDING, R. MILLS, **Trace-Ion Diffusion in Molten Alkali Carbonates,** J. Electrochem. Soc., 112 (1965) 594-599.

[10] P.L. SPEDDING, R. MILLS, **Tracer Diffusion Measurements in Mixtures of Molten Alkali Carbonates,** J. Electrochem. Soc., 113 (1966) 599-603.

[11] W. ZHU, C. XIA, D. DING, X. SHI, G. MENG, **Electrical properties of ceria-carbonate composite electrolytes,** Mater. Res. Bull., 41 (2006) 2057-2064.

[12] A. EVANS, W. XING, T. NORBY, **Electromotive Force (emf) Determination of Transport Numbers for Native and Foreign Ions in Molten Alkali Metal Carbonates,** J. Electrochem. Soc., 162 (2015) F1135-F1143.

[13] H. NÄFE, **Electrochemical CO_2 Separation through an Alkali-Carbonate-Based Membrane,** ECS J. Solid State Sci. Technol., 3 (2014) N23-N29.

[14] P.L. SPEDDING, **Electrical conductance of molten alkali carbonate binary-mixtures,** J. Electrochem. Soc., 120 (1973) 1049-52.

[15] T. KOJIMA, Y. MIYAZAKI, K. NOMURA, K. TANIMOTO, **Electrical conductivity of molten Li_2CO_3-X_2CO_3 (X: Na, K, Rb, and Cs) and Na-$_2CO_3$-Z_2CO_3 (Z: K, Rb, and Cs)**, J. Electrochem. Soc., 154 (2007) F222-30.

[16] B.C.H. STEELE, **Appraisal of $Ce_{1-y}Gd_yO_{2-y/2}$ electrolytes for IT-SOFC operation at 500 °C**, Solid State Ionics, 129 (2000) 95-110.

[17] F.M.L. FIGUEIREDO, F.M.B. MARQUES, **Electrolytes for solid oxide fuel cells**, Wiley Interdisciplinary Reviews: Energy and Environment, 2 (2013) 52-72.

[18] J.L WADE, K.S. LACKNER, A.C. WEST, **Transport model for high temperature, mixed conducting CO_2 separation membranes**, Solid State Ionics, 178 (2007) 1530-1540.

[19] Z. RUI, M. ANDERSON, Y.S. LIN, Y. LI, **Modeling and analysis of carbon dioxide permeation through ceramic-carbonate dual-phase membranes**, J. Memb. Sci., 345 (2009) 110-118.

[20] J. ORTIZ-LANDEROS, T. NORTON, Y.S. LIN, **Effects of support pore structure on carbon dioxide permeation of ceramic-carbonate dual-phase membranes**, Chem. Eng. Sci., 104 (2013) 891-898.

[21] F.M.B. MARQUES, S.G. PATRÍCIO, E. MUCCILLO, R. MUCCILLO, **On the Model Performance of Composite CO_2 Separation Membranes**, Electrochim. Acta, 210 (2016) 87–95.

[22] S.G. PATRÍCIO AND F.M.B. MARQUES, **Benchmarking the ambipolar conductivity of composite electrolytes for gas separation membranes**, Int. J. Energ. Res. (2016) DOI: 10.1002/er.3596.

[23] C.M.C SOARES, S.G. PATRÍCIO, F.M.L. FIGUEIREDO, F.M.B. MARQUES, **Relevance of the ceramic content on dual oxide and carbonate-ion transport in composite membranes**, Int. J. Hydrogen Energ. 39 (2014) 5424-32.

[24] A.I.B. RONDÃO, S.G. PATRÍCIO, F.M.L. FIGUEIREDO, F.M.B. MARQUES, **Composite electrolytes for fuel cells: Long-term stability under variable atmosphere**, Int. J. Hydrogen Energ., 39 (2014) 5460-69.

[25] A.I.B. RONDÃO, S.G. PATRÍCIO, F.M.L. FIGUEIREDO, F.M.B. MARQUES, **Role of gas-phase composition on the performance of ceria-based composite electrolytes**, Int. J. Hydrogen Energ., 38 (2013) 5497-5506.

[26] J. SUNARSO, S. BAUMANN, J.M. SERRA, W.A. MEULENBERG, S. LIU, Y.S. LIN, J.C. DINIZ DA COSTA, **Mixed ionic–electronic conducting (MIEC) ceramic-based membranes for oxygen separation**, J. Memb. Sci., 320 (2008) 13-41.

[27] J. TONG, L. ZHANG, M. HAN, K. HUANG, **Electrochemical separation of CO_2 from a simulated flue gas with high-temperature ceramic–carbonate membrane: New observations**, J. Membr. Sci., 477 (2015) 1-6.

[28] S.G. PATRÍCIO, E. PAPAIOANNOU, G. ZHANG, I.S. METCALFE, F.M.B. MARQUES, **High performance composite CO_2 separation membranes**, J. Membr. Sci., 471 (2014) 211–218.